ENHANCEMENT OF COMBINED HEAT AND MASS TRANSFER IN ROTARY EXCHANGERS

U. DINGLREITER, F. MAYINGER
Lehrstuhl A für Thermodynamik
Technische Universität München
Boltzmannstraße 15
D-85748 Garching, Germany

Abstract. The principal objective of this study is the analysis and improvement of the combined heat and mass transfer of various newly designed rotary solid storage elements.

Rotary exchangers usually consist of a combination of a carrying material and an adsorbing storage element. The heat and mass transfer surface is of cellular structure usually referred to as matrix. Using the holographic interferometry experiments were conducted in order to determine the most effective duct geometry for advanced heat and mass transfer. Therefore various duct geometries like sinusoidal, rectangular, triangular and semicircular ducts were investigated at different temperatures and flow velocities. According to the configurations that were examined experimentally a numerical calculation has been performed.

In order to improve the heat and mass transfer in rotary exchangers several new combinations of carrying materials and adsorbents were developed and compared to a reference material. Ten combinations which proved to be most effective were scrutinized. For this reason the water adsorption and regeneration behavior as well as the pressure drop was measured. Cycle experiments were conducted in order to determine the suitability of a material combination as a rotary humidity exchanger. The results demonstrate a good applicability of most of the new materials.

1. Introduction

Rotary solid storage elements are used in a great multitude of technical processes such as air dehumidification or solvent recovery. The design showing the best prospects is the rotary counter flow conception which combines high performance with compactness. The regenerator generally consists of a matrix of flow channels which have, depending on the manufacturing process, a rectangular, triangular or sinusoidal shape. The disk exchanger is separated by flow channels into two sections, the regeneration section and the adsorption section, in which the process air and the regeneration air are

S. Kakaç et al. (eds.), Heat Transfer Enhancement of Heat Exchangers, 381–394.
© 1999 *Kluwer Academic Publishers. Printed in the Netherlands.*

in counter flow with the matrix. In the adsorption section the adsorbate (humidity or solvent) from the air is stored to the matrix walls, whereas the preheated air passing through the regeneration section of the rotor heats up the material and regenerates it. After several revolutions a steady state with a constant mass transfer from adsorption air to regeneration air is achieved. The volume flow through the regeneration area is about a quarter of the volume flow through the adsorption area. For this reason the humidity or the solvents are considerably more concentrated in the regeneration air. This results in a better performance of a condensation procedure or a catalytic oxidation.

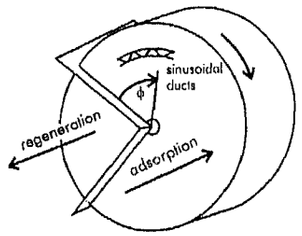

Figure 1. Rotary mass exchanger

For the development of further appropriate adsorbens-carrying material combinations, firstly the influence of the geometry of the flow channels and of the flow velocity on the heat transfer was investigated at various temperatures. Considering the opposite direction of the heat and the mass transfer in the adsorption process, the analogy between heat and mass transfer can be used to determine the mass transfer coefficient (Krischer [1]). Both the heat transfer coefficient and the mass transfer coefficient are required as input data to perform a numerical simulation of the combined heat and mass transfer in rotary exchangers. Subsequently samples of various new material combinations and geometries were manufactured and investigated with respect to their suitability as rotary humidity exchangers. The adsorption and regeneration behavior as well as the pressure drop were investigated. By means of cycle experiments the applicability of the new materials could be determined.

2. Rotary Exchanger Duct Geomtries

Three main aspects have to be considered when designing single ducts in the rotary adsorbers:

- heat and mass transfer
- pressure drop
- producibility

As a first step the literature (e.g., Shah and London, [10] [11]) provides data on mean heat transfer and pressure drop in ducts with different cross sectional geometries for fully developed laminar flow and allows a pre-selection of duct cross-sectional geometries.

In order to get detailed information about the local heat transfer in the duct, also for higher flow rates (especially in the transition region from laminar to turbulent flow) and the combined (thermal and velocity) entry length problem, additional experiments and numerical calculations have been performed.

duct geometry	2b/2a (height/bottom)	Nu_T	Nu_{H1}	L_{hy}^+	ζRe
rectangular	1,00	2,98	3,61	0,0340	56,91
circular	1,00	3,66	4,36	0,0500	64,00
semicircular	0,50	---	4,09	---	63,07
sinusoidal	0,50	2,12	2,62	0,0464	44,83
sinusoidal	0,56	2,17	2,69	0,0453	45,81
sinusoidal	0,64	2,24	2,78	0,0439	47,13
sinusoidal	0,68	2,27	2,83	0,0432	47,79
sinusoidal	1,00	2,45	3,10	0,0400	52,09
sinusoidal	1,50	2,60	3,27	0,0394	56,09
triangular (60°)	0,86	2,47	3,11	0,0398	53,33
triangular (90°)	0,50	2,34	2,98	0,0421	52,61

TABLE I. Heat Transfer (Nu_T: T_W=const. Nu_H: q = const.) and pressure drop coefficient ζRe for fully developed, laminar flow (Shah und London, [10]). Hydrodynamical entry length L_{hy}^+ for various channel geometries

2.1. EXPERIMENTAL SET-UP FOR HOLOGRAPHIC INTERFEROMETRY

The influences of the duct geometry and of the flow velocity on heat transfer were investigated at various temperatures by holographic interferometry. Ambient air from the climate controlled laboratory (T_∞ = 20°C) is drawn directly into the test section by means of a compressor which is equipped with a flow-regulating throttle. Considering the original rotary adsorber arrangement no inlet sections or any flow homogenizers are applied to the duct. The test section consists of a heated aluminum duct with uniform wall temperature. The duct outlet is connected to a funnel with glass walls that allows optical access in the axial direction of the duct, which is also the main flow direction (figure 2b).

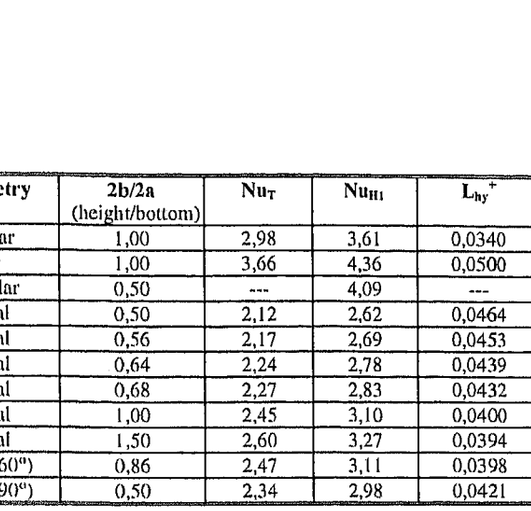

Figure 2. a) Setup for holographic interferometry (real-time)
b) Setup for the investigation of single ducts

Two-dimensional temperature fields, and thus the local heat transfer in the duct, were obtained by holographic interferometry measurements. The experimental set-up for the holographic interferometry (real-time method) is illustrated in figure 2a. This optical measurement technique allows the continuous visualization of the two-dimensional temperature field in the flow, avoiding any influence on the effect to be measured. This technique shows the thermohydraulic flow pattern within the duct in real time. Detailed information about this measurement technique and its applications are given by Mayinger et al. [4], [5],[6],[7] and Tauscher and Mayinger [12]. For the basic understanding of the interferograms presented in this paper (figures 3 and 4) it is only important to mention, that the interference lines (black and white fringes in the images) of the interferograms are approximately equal to the isotherms of the investigated flow (temperature step: $\Delta T = 2.3$ K). Due to the experimental set-up these isotherms represent the axially integrated temperature in the duct. From the distance between these isotherms and the known wall temperature, the temperature gradient and, therefore, the local heat flux, the local heat transfer coefficient and the local Nusselt number can be calculated. For the evaluation of the interferograms, such as the measurements of the fringe distances along lines which are perpendicular to the wall, a home made digital image processing system was used.

In table 2 the experimentally investigated arrangements are shown. Due to space restrictions only the most important results concerning local heat transfer will be presented in the following.

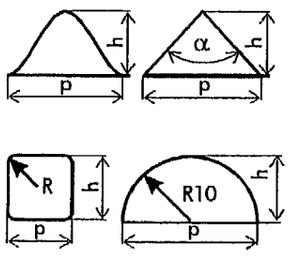

duct geometry:		Variation
sinusoidal:	h/p:	0,54 / 0,56 / 0,68 / 1,00 / 1,50
rectangular:	R:	1 / 3 / 5 mm
triangular:	h/p:	1,12; α=60° / 0,5; α=90°
semicircular:	h/p:	0,5
length:	L:	100 / 200 / 300 mm
wall temperature:		30 / 50 / 70 / 90 °C
Reynolds number:		50 – 50 000

TABLE 2. Experimentally investigated arrangements

2.2. EXPERIMENTAL RESULTS

Figures 3 and 4 show interferograms of the air flow in different sinusoidal, semicircular, triangular and rectangular ducts at different Reynolds numbers.

It is apparent that the flow temperature gradient reaches the highest values in linear perimeter sections, while minima can be observed in the corners. With increasing the flow rates the air flow is able to reach also corners and to use also these duct areas for heat transfer. As mentioned above the local Nusselt number over the duct perimeter is obtained by evaluating the interferograms. An exemplary evaluation is shown in figure 5. By integrating the local heat transfer the mean heat transfer for each duct is gained. This can be used to verify the measurements by comparing them to global calorimetric measurements.

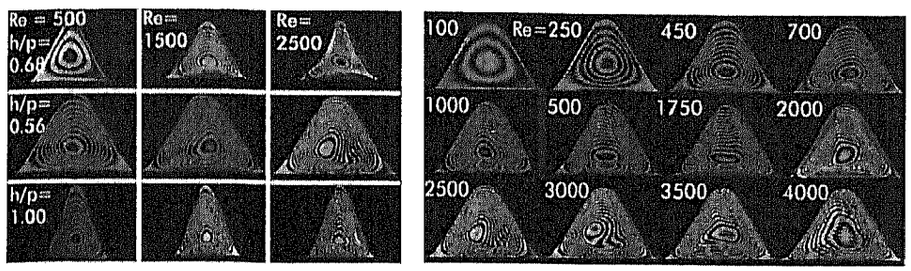

Figure 3. Temperature field in sinusoidal ducts at different Reynolds numbers

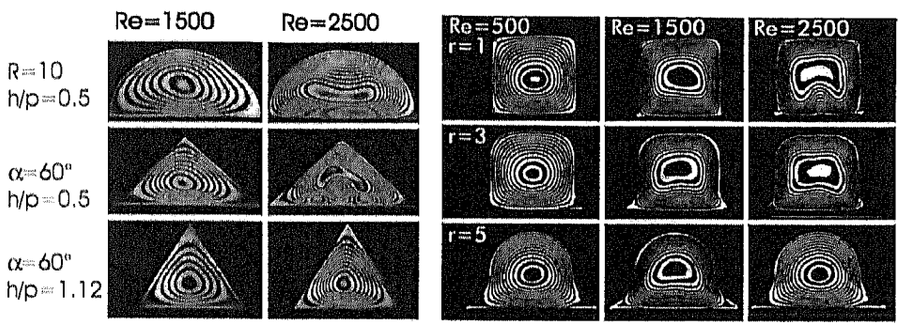

Figure 4. Temperature field in semicircular, triangular and rectangular ducts at different Reynolds numbers

Due to the fact that the optical experiments are very time consuming, also numerical calculations have been performed (figure 6). Once the numerical results have been verified by the experimental data, further parameter variations can be supplied by computer only. The numerical simulation of the fluid flow in the ducts was performed by means of the commercially available CFD-code CFX. This code works with a finite volume method based on the finite elements. The boundary conditions and the geometry were modeled exactly as in the experimental set-up.

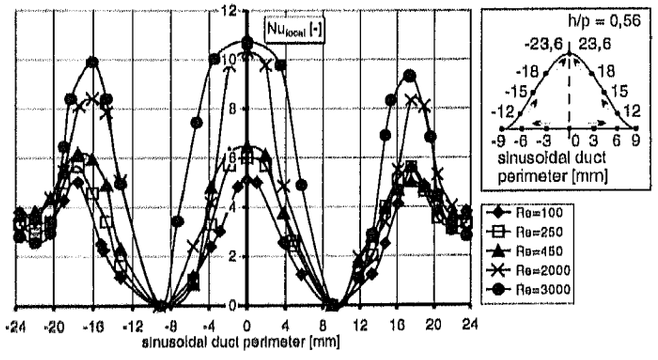

Figure 5. Local Nusselt number over sinusoidal duct perimeter

The symmetry of the ducts was used to model only one half of the duct in order to increase the calculation speed. The difference between the numerical calculation and

the experimental results is less than 12% for each Reynolds number. The experimental mean Nusselt numbers have always a lower value than the ones which are calculated. This behavior becomes evident when regarding the trends of the local Nusselt numbers. Although the maxima in the experimental Nusselt numbers are slightly higher than the calculated ones, they are not that great. This results possibly from the fact, that, due to limitations of the digital image processing system, only few temperature gradients have been evaluated along the duct perimeter.

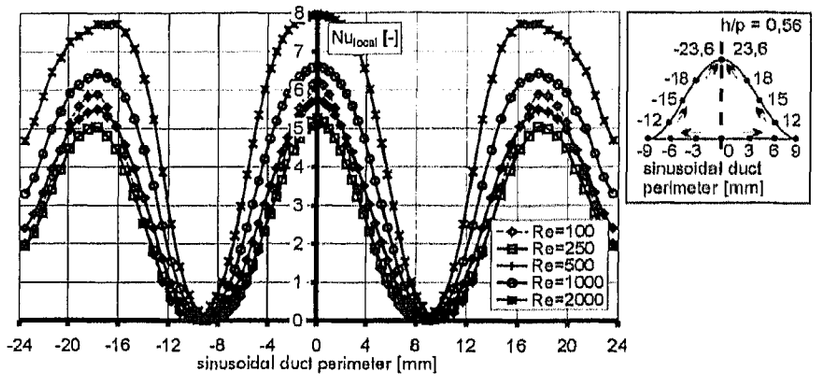

Figure 6. Local Nusselt number for a sinusoidal duct (h/p = 0.56) obtained from simulation

An additional fact is that the axial progression of the heat transfer coefficient, which is required for the numerical calculation of the combined heat and mass transfer of rotary exchangers, is a result of the numerical simulation. In figure 7 the perimeter averaged Nusselt number is depicted.

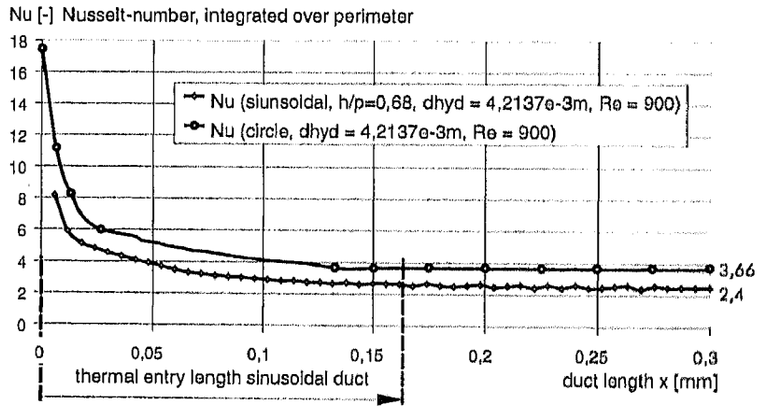

Figure 7. Nusselt number integrated over perimeter for circular and sinusoidal duct

As a result of these experiments and calculations for each duct geometry, best practice parameters were obtained.
For sinusoidal ducts a height to bottom length ratio of 0,6 up to 0,7 is most effective.

3. Investigation of Rotary Exchanger Samples

3.1. ROTARY EXCHANGER SAMPLES

sample	description	duct geometry	manufacturer	cross section [dm^2]	number of ducts
1P	silicagel-coated. adsorption paper	sinusoidal small	Lehrstuhl A für Thermodynamik	0,32	1160
2P	silicagel-coated. adsorption paper	sinusoidal medium	Lehrstuhl A für Thermodynamik	0,31	730
3P	adsorption paper not coated.	sinusoidal medium	Lehrstuhl A für Thermodynamik	0,30	705
4P	silicagel-coated. adsorption paper	sinusoidal large	Lehrstuhl A für Thermodynamik	0,29	333
K1	synthet. silicagel-on ceramic	sinusoidal medium	reference material	0,32	1057
K2	ceramic, LiCL-coated	rectangular	R. Scheuchl GmbH	0,32	1884
Z1	extruded zeolite (monolith)	rectangular	IKT (Stuttgart University)	0,32	1952
Z2	zeolite-coated adsorption paper	sinusoidal medium	Lehrstuhl A für Thermodynamik	0,31	712
Z3	zeolite-coated. adsorption paper	sinusoidal medium	Lehrstuhl A für Thermodynamik	0,30	733
Li I	adsorption paper LiCl-coated	sinusoidal medium	Lehrstuhl A für Thermodynamik	0,29	626

TABLE 3. Characterization of the rotary exchanger samples

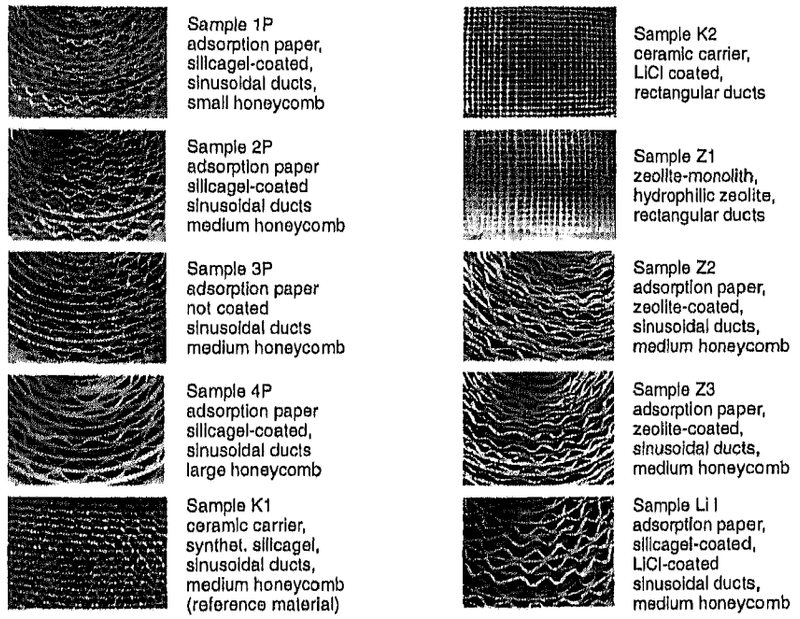

Figure 8. Investigated rotary exchanger samples

In order to gain information about the pressure drop, the loading capabilities and regenerability of several different material combinations, rotary exchanger samples with a diameter of 70mm and a duct length of 200mm were designed. In the following experiments ten different combinations of carrying structures and adsorbents as shown in figure 8 were investigated. Table 3 characterizes the different samples referring to duct geometry, manufacturer, cross section and number of ducts.
Most of the samples consist of a new non-flammable adsorption paper which was developed at Lehrstuhl A für Thermodynamik. In order to improve the adsorption properties the production process of conventionally used non flammable paper was modified. This modification leads to a silicagel portion of almost 50% in the paper itself. For some applications the portion of adsorbents is increased by an additional silicagel, zeolite or LiCl-coating. In figure 9 SEM-pictures of a conventional paper, of the modified adsorption paper, and of the adsorption paper after an additional silicagel coating are shown.

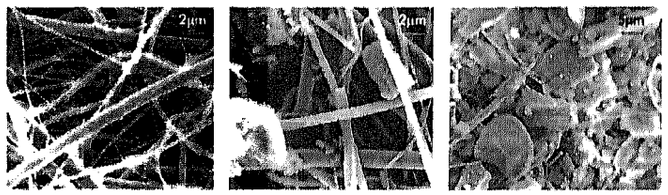

Figure 9. SEM-Pictures of conventional non flammable paper (left), adsorption paper (middle) and additionally coated adsorption paper (right)

The samples 1P, 2P, 4P differ only in the dimensions of the sinusoidal duct. There is no difference in the coating. Sample 3P consists of uncoated adsorption paper, whereas sample LI I was first coated with silicagel and afterwards soaked in a 13% LiCl-solution. Sample K1 was bought and serves as a reference material to the newly developed combinations. Sample K2 consists of a extruded ceramic carrier that was soaked in the LiCl-solution. Together with sample K2 the ducts of sample Z1 are rectangular. Sample Z1 consists of a extrudated hydrophilic zeolite. It was developed at the Institut für Kunststofftechnologie, Universität Stuttgart and placed at our disposal for further measurements. The samples Z2 and Z3 are adsorption papers coated with different, hydrophilic molecular sieves.

3.2. EXPERIMENTAL SET-UP

Figure 10 shows the following experimental rig which was used for the investigation of the combined heat and mass transfer in rotary exchanger samples.

The holding device for the sample is composed of a tube jointing sleeve with a diameter of 70 mm and a length of 220 mm in which the sample is inserted. The air temperature and the humidity are adjusted in a conditioning section. Thermocouples and humidity sensors for the determination of the air temperature and humidity are positioned at a short distance in front of and after the rotary exchanger sample.

Along a surface line in a flow channel of the sample there are seven thermocouples arranged at an equal distance from one another. They measure the temperature distribution in the sample during the adsorption or desorption process. By means of a high-accuracy weighing machine the loading progression of the sample can be measured.

The experimental rig enables the investigation of sample diameters up to 70 mm and of flow velocities up to 10 m/s. Inlet-temperatures between 0°C and 80°C and air humidity up to 98 % at a temperature of 45°C can be adjusted.

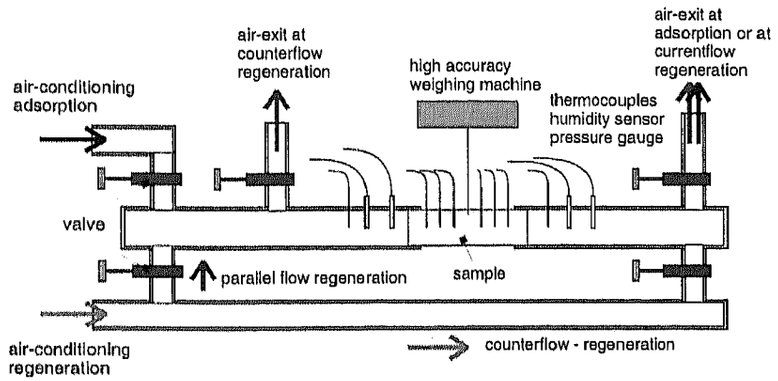

Figure 10. Experimental rig for the investigation of rotary exchanger samples

Before an experiment is conducted the samples are dried in a vacuum oven (pressure < 100 mbar) at a temperature of 130°C for at least 24 hours.
By measuring the pressure drop and the adsorption isotherms a first evaluation of the loading behavior of the samples can be realized. The regeneration behavior of the material combinations is then investigated. In order to prove the suitability of a material as a rotary exchanger, several cycle-experiments were conducted.

3.3. PRESSURE DROP OF THE SAMPLES

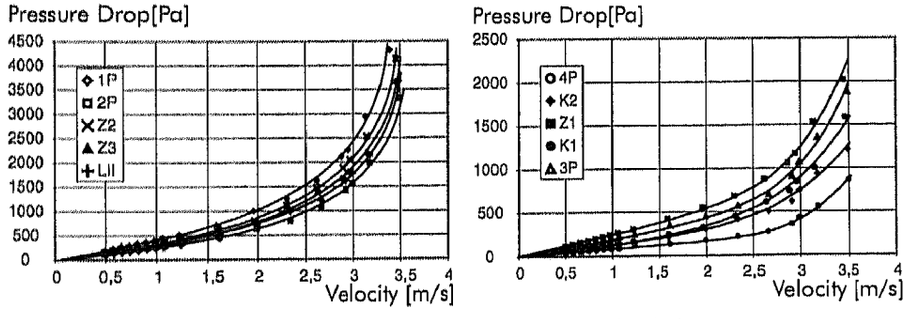

Figure 11. Pressure loss of all samples versus air velocity

In order to avoid high pumping power, duct geometries with a maximum in mass transfer combined with minimum in pressure drop have to be developed. In figure 11

the pressure drops of all samples are shown. In the important velocity range up to 2m/s the pressure drop of the samples depicted in the right graph are comparable to that pressure drop of the reference sample K1 which has the lowest of all samples. The pressure drop of the samples 1P, 2P, Z2, Z3 and Li I is significantly higher. This is due to smaller honeycomb ducts together with a thick coating with silicagel or molecular sieve.

3.4. ADSORPTION EQUILIBRIUM

In order to get detailed information about the adsorption behavor the adsorption isotherms for air temperatures of 25°C, 35°C, 45°C and 55°C at relative humidities from 0% to 90% were measured.

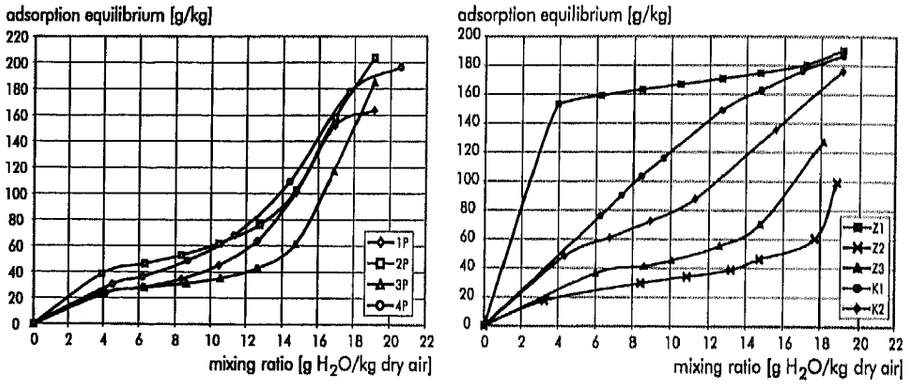

Figure 12. Adsorption isotherms at a temperature of 25°C

In figure 12 the 25°C-isotherms are presented for all samples except for the sample Li I. The isotherm of this material exceeds the scale in a linear way up to a equilibrium of about 1600g water/kg dry material at a mixing ratio of 16g water/kg dry air.

The adsorption isotherm of the sample Z1 rises steeply up to a proportion of ingredients of 5kg water per kg dry air and then rises steadily until it reaches the maximum loading (19.05%). The progression of the reference sample is characterized by a steady rise up to the maximum loading of approximately 19.0%. The isotherm of sample K2 shows almost the same behavior, with a slight decrease at the mixing ratio between those of 5 and 12g/kg. The adsorption paper based samples (1P, 2P, 3P, 4P, Z2 and Z3) show a similar progression with a flattening at a mixing ratio of 4 to 5 g/kg and a steep increase at a mixing ratio of approximately 12 to 14 g/kg.

All material combinations show good adsorption behavior.

3.5. REGENERATION BEHAVIOR

In addition to the adsorption capabilities the regeneration behavior is to be considered.

Therefore, in the experimental setup depicted in figure 9 the samples underwent the following measurement cycle:

- regeneration — until the samples are dry (24 hours in a vacuum oven 130°C)
- adsorption — air flow 30°C, 60% relative humidity, 1m/s, 20 minutes
- regeneration — air flow 130°C, 0% relative humidity, 1m/s, 20 minutes
- adsorption — air flow 30°C, 60% relative humidity, 1m/s, 10 minutes
- regeneration — air flow 130°C, 0% relative humidity, 1m/s, 10 minutes

The results of these investigation are presented in figure 13. The samples which consist of the new adsorption paper (left graph: all samples, right graph: sample Z3) except the sample Li I reach their dry mass at least within the first half of the regeneration time. Within a quarter of the regeneration time the loading of sample 4P decreases below 15%, the loading of the other adsorption paper samples decreases below 5% of their maximum loading. Compared to the reference (sample K1) these results indicate good suitability. By means of a high heat capacity the regeneration behavior of sample Z1 is inadequate for usage in a cycle process with high frequencies. Within the full time range it is not possible to regenerate this sample to its dry mass.

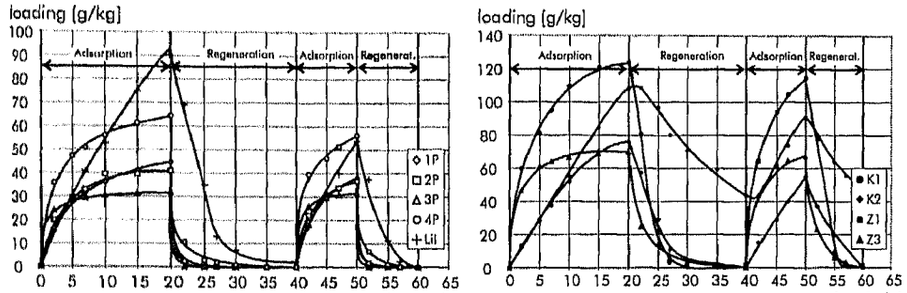

Figure 13. Regeneration behavior after 20min and after 10min water adsorption

3.6. CYCLE EXPERIMENTS

In the cycle process the matrix is frequently loaded and regenerated. In order to concentrate humidity or solvent in the regeneration air, the regeneration period is usually reduced to a quarter of the adsorption period. According to literature the optimal number of revolutions of rotary mass exchangers is between 18 and 25. For the reference material (sample K1) an efficient number of revolutions of 24 was investigated. Therefore, for each duct a retention time in the adsorption area of 112,5 seconds is obtained, whereas in the regeneration area the retention time is 37,5 seconds. In order to determine the applicability in comparison to the reference sample under these conditions, all newly designed material combinations were investigated in a cycle experiment. In the adsorption period air with a velocity of 1m/s, a temperature of 30°C and a relative humidity of 60% flows through the sample within 112,5 seconds. After the sample has been weighed, the regenerating air, with a velocity of 1m/s, a temperature of 130°C and a relative humidity of 0%, flows in the opposite direction through the sample for another 37,5 seconds. Afterwards the sample is weighed again and the cycle starts at the beginning. In advance the samples were dried in the vacuum oven at a temperature of 130°C.

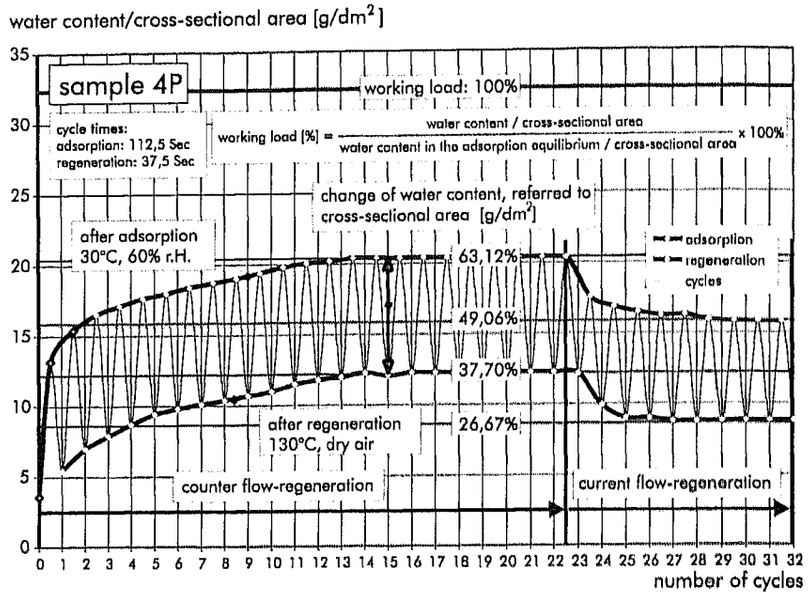

Figure 14. Cycle experiment of sample 4 – Explanation of table 4 and table 5

Cycle-Experiments	adsorption:	112,5 sec	30°C	60% r.H.	1m/s					
	regeneration:	37,5 sec	130°C	0% r.H.	1m/s					
counter flow-regeneration	sample	1P	2P	3P	4P	K1	K2	Z1	Z3	Li I
	number of cycles	9	9	5	14	15	16	20	13	130
	absolute water content[g]	1,66	1,75	1,69	2,41	2,48	2,10	1,55	1,92	1,45
	change in loading [g/kg]	13,05	14,43	20,90	22,99	15,29	6,17	4,89	15,77	8,17
	water change/cross section [g/dm²]	5,16	5,60	5,56	8,22	7,78	6,54	4,81	6,31	4,93
	working load after adsorption [%]	49,35	47,17	85,70	63,12	95,21	78,56	97,16	76,72	50,14
	working load after regeneration [%]	28,78	27,84	36,35	37,70	84,61	72,71	94,23	48,10	49,40
parallel flow-regeneration	sample	1P	2P	3P	4P	K1	K2	Z1	Z3	Li I
	number of cycles	7	4	1	6	9	7	9	5	---
	absolute water content[g]	0,93	1,28	1,59	2,13	2,15	1,40	1,15	1,20	---
	change in loading [g/kg]	7,32	10,58	19,61	20,25	13,25	4,11	3,63	9,91	---
	water change/cross section [g/dm²]	2,89	4,10	5,22	7,24	6,74	4,36	3,57	3,96	---
	working load after adsorption [%]	33,39	35,99	83,90	49,06	62,18	45,13	90,64	59,16	---
	working load after regeneration [%]	21,86	21,82	37,61	26,67	52,99	41,23	88,47	41,18	---

TABLE 4. Cycle experiment: all samples, counter flow and parallel flow-regeneration; adsorption at 30°C, 60% r.H.

The cycle was repeated until a steady state was obtained. Then the cycle experiments were continued with a current flow regeneration until a new steady state was reached.

The most important criterion for the application as a rotary exchanger is the change in the water content related to the flow surface of the material between adsorption and regeneration.

In addition to that change of the water content, the number of cycles to steady state, the absolute water content, the change of loading and the working load are listed in table 4 and table 5 for counter flow and parallel flow regeneration and for different regeneration air humidities. The listed sizes are explained in figure 14 with sample 4P as an example.

Cycle-Experiments	adsorption:	112,5 sec	30°C	80%/30% r.H.	1m/s
	regeneration:	37,5 sec	130°C	0% r.H.	1m/s
adsorption at a relative humidity of 80% counter flow-regeneration	sample			4P	K1
	number of cycles (steady state)			14	15
	absolute water content [g]			2,41	2,48
	change in loading [g/kg]			22,99	15,29
	water change/cross section [g/dm²]			8,22	7,78
	working load after adsorption [%]			63,12	95,21
	working load after regeneration [%]			37,70	84,61
adsorption at a relative humidity of 30% parallel flow-regeneration	sample			4P	K1
	number of cycles (steady state)			6	9
	absolute water content [g]			2,13	2,15
	change in loading [g/kg]			20,25	13,25
	water change/cross section [g/dm²]			7,24	6,74
	working load after adsorption [%]			49,06	62,18
	working load after regeneration [%]			26,67	52,99

TABLE 5. Cycle experiment: samples 4P, K1, counter flow and parallel flow-regeneration; adsorption at 30°C, 80% r.H and 30% r.H.

Table 4 shows a maximum of the water change over all samples of 8.22g/dm² for sample 4P. According to the water change of the reference sample K1 (7,78) an improvement of approximately 5,66% was achieved. Considering all relative humidities of the adsorption air (table 5), sample 4P shows better values than the reference sample. In industrial applications a water change related to a cross section of about 5g/dm² at the adsorption air temperature of 30°C and a humidity of 60% is used to calculate the device. Only the samples Z1 and Li I do not achieve this value. For these two samples the cycle has to be modified to lower cycle frequencies and maybe to a higher adsorption to regeneration time relation.

4. Concluding Remarks

Several different duct geometries were investigated by means of holografic interferometry. Due to manufacturing requirements all adsorption-paper-based materials

should have a matrix with sinusoidal ducts. The value of the height-to-bottom length ratio should be between 0,6 and 0,7. In addition to the optical experiments the numerical simulation of the heat transfer provides values for the mean axial heat transfer coefficient. With respect to the analogy between heat and mass transfer, the mass transfer coefficient can be obtained additionally. Both values are required for a numerical simulation of the combined transport processes concerning rotating exchangers. This simulation serves as an important tool for the design of industrial devices.

Most of the new material combinations show good performance in the cycle experiments, which represents a relevant test for the application of rotary exchangers. Additionally, the mechanical properties of all samples are very satisfactory. As a consequence of the presented results a serial production of rotary exchangers has started. The exchangers are used as dehumidifiers particularly in desiccant cooling systems or other industrial applications.

The modified production process of the adsorption paper and the following coating process allow the production of hydrophobic exchanger materials as well. The portion of hydrophilic and hydrophobic adsorbents is variable in a wide range. This fact enables the design of rotary exchangers for both dehumidification and solvent recovery in a single device.

There is a need for further research in order to optimize the material combination, as well as the geometry according to each application.

5. References

1. O. Krischer, W. Kast (1978) Die wissenschaftlichen Grundlagen der Trocknungstechnik, Dritte Auflage, *Springer Verlag*, Berlin
2. Hauff, W., Grigull, U., Mayinger, F. (1991) Optische Meßverfahren in der Wärme- und Stoffübertragung, *Springer-Verlag*, Berlin
3. Klas, J. (1993) Wärmeübergang in Strömungskanälen ohne und mit Turbulenzpromotoren *Diss.* TU-München
4. Mayinger, F. (Ed..) (1994) Optical Measurements, Techniques and Applications, *Springer-Verlag*, Berlin
5. Mayinger, F., Chen, Y.M. (1985) Holographic Interferometry Studies of the Temperature Field Near a Condensing Bubble, Optical Methods in Dynamics of Fluids and Solids, *Proc. of an Int. Symposium IUTAM*, Berlin
6. Mayinger, F., Klas, J. (1993) Investigation of Local Heat Transfer in Compact Heat Exchangers by Holographic Interferometry, *Proc. of the 1st Int. Conf. on Aerospace Heat Exchanger Technology*, pp. 449-465, Palo Alto
7. Mayinger, F., Panknin, W. (1994) Holography in Heat and Mass Transfer , *Proc. of the 5th Int. Heat Transf. Conf.*, Tokyo
8. Panknin, W., Mayinger, F. (1978) Anwendung der holographischen Zweiwellenlängeninterferometrie zur Messungüberlagerter Temperatur- und Konzentrationsgrenzschichten, *Verfahrenstechnik*, Bd. 12,9, pp. 582-589
9. C.P. Howard (1965) Heat Transfer and Flow-Friction Characeristics of Skewed-Passage and Glass-Ceramic Heat-Transfer Surfaces,
   Int. Journal Heat Mass Transfer - Oxford 1. S 72-86
10. Shah, R.K., London, A.L. (1978) Laminar Flow Forced Convection in Ducts
    Academic Press, New York
11. R.K. Shah (1981) Thermal Design Theory for Regenerators,
    Heat Exchangers, Thermal Hydraulic Fundamentals and Design, edited by S. Kakac, A.E. Bergles and F. Mayinger, pp. 721 - 763, *Hemisphere*, New York
12. Tauscher, R., Mayinger, F. (1997) Advances in Heat Transfer by Optical Techniques, *Proc. of the 2nd Int. Symposium on Heat Transfer and Energy Conservation*, Guangzhou, pp.14-29